REFLECTION MOVEOUT INVERSION FOR HORIZONTAL TRANSVERSE ISOTROPY: ACCURACY AND LIMITATION

AbdulFattah Al-Dajani

Earth Resources Laboratory
Department of Earth, Atmospheric, and Planetary Sciences
Massachusetts Institute of Technology
Cambridge, MA 02139

Tariq Alkhalifah

Stanford Exploration Project
Dept. of Geophysics
Stanford University
Stanford, CA 94305

ABSTRACT

Horizontal transverse isotropy (HTI) is the simplest azimuthally anisotropic model used to describe vertical fracturing in an isotropic matrix. Using the elliptical variation of P–wave normal-moveout (NMO) velocity with azimuth, measured in three different source-to-receiver orientations, we can obtain the vertical velocity V_{Pvert}, anisotropy parameter $\delta^{(\mathrm{V})}$, and the azimuth α of the symmetry-axis plane.

Parameter estimation from variations in the moveout velocity in azimuthally anisotropic media is quite sensitive to the angular separation between the survey lines in 2D, or equivalently source-to-receiver azimuths in 3D, and to the set of azimuths used in the inversion procedure. The accuracy in estimating the parameter α, in particular, is also sensitive to the strength of anisotropy. The accuracy in resolving $\delta^{(\mathrm{V})}$ and V_{Pvert} is about the same for any strength of anisotropy. In order to maximize the accuracy and stability in parameter estimation, it is best to have the azimuths for the three source-to-receiver directions 60° apart. In land seismic data acquisition having wide azimuthal coverage is quite feasible. In marine seismic data acquisition, however, where the azimuthal data coverage is limited, multiple survey directions are necessary to achieve such wide azimuthal coverage.

Having more than three distinct source-to-receiver azimuths (e.g., full azimuthal coverage) provides useful data redundancy that enhances the quality of the estimates, and sets the stage for a least-square type of inversion in which the errors in the parameters estimates are minimized in a least-square sense.

In layered azimuthally anisotropic media, applying Dix differentiation to obtain interval moveout velocity provides sufficient accuracy in the inversion for the medium parameters, especially where the direction of the symmetry planes is uniform. In order to obtain acceptable parameter estimates, an HTI layer overlain by an azimuthally isotropic overburden (as might happen for fractured reservoirs) should have a thickness (in time) relative to the total thickness. The total thickness should be equal to or greater than the ratio of the error in the NMO (stacking) velocity to the interval anisotropy strength of the fractured layer.

INTRODUCTION

The model of transverse isotropy with horizontal symmetry-axis (HTI medium) is the simplest azimuthally anisotropic model used to describe vertically fractured reservoirs. The two orthogonal vertical symmetry planes that characterize the HTI model are: the symmetry-axis plane, which contains the symmetry-axis (perpendicular to the cracks) and the isotropy plane (parallel to the cracks). The HTI model also is described by the Thomsen (1986) parameters of an equivalent vertical transverse isotropic (VTI) medium that generates the same wave-propagation signatures in the symmetry-axis plane as in the original HTI medium. These parameters, defined with respect to the vertical axis, govern the moveout for HTI media, even outside the symmetry-axis plane where the equivalence between the two models is not valid (Tsvankin, 1995; Al-Dajani and Tsvankin, 1996). The equivalent VTI Thomsen parameters are $\epsilon^{(V)}$, $\delta^{(V)}$, and $\gamma^{(V)}$, in addition to the vertical P- and S-velocities (Rüger, 1995).

The presence of azimuthal anisotropy in practice has been documented in several studies, such as those by Lynn *et al.* (1995) and Mallick *et al.* (1996). With increased use of multicomponent seismic surveys and with close attention paid to fractured-reservoir characterization in making hydrocarbon drilling and production decisions, azimuthal anisotropy has attracted the interest of researchers (e.g., Crampin *et al.*, 1980; Thomsen, 1988, 1995; Sena, 1991; Rüger, 1995; Tsvankin, 1995, 1997; Al-Dajani and Tsvankin, 1996.)

Tsvankin (1995) derived an analytic expression for the short-spread NMO velocity that is valid for pure mode propagation and arbitrary strength of anisotropy in a single-homogeneous HTI layer with a horizontal reflector. The elliptical variation of this NMO velocity as a function of azimuth, in the horizontal plane, is not only restricted to HTI media, but also occurs for media with more general azimuthal anisotropy (e.g., orthorhombic) (Grechka and Tsvankin, 1996). In their study of reflection moveout in HTI media, Al-Dajani and Tsvankin (1996) derived an exact analytic expression for the quartic coefficient of the Taylor's series expansion of the traveltime-offset curves. This

expression is valid for pure mode propagation and arbitrary strength of anisotropy.

The inversion for the parameters of azimuthally anisotropic media has been limited mostly to shear-wave splitting analysis with the goal of estimating crack orientation and crack density. One of the few parameter-estimation algorithms based on moveout analysis of P-wave data was presented by Sena (1991); however, Sena's method is limited to weak anisotropy and requires knowledge of the vertical velocity.

Here, we discuss the estimation of anisotropic parameters and the detection of fracture orientation from reflection moveout data in homogeneous and horizontally-layered HTI media. Estimating the anisotropy parameters allows the possibility of estimating a quantity for crack density, in addition to estimating crack orientation, of great interest in the characterization of fractured reservoirs. The error study here provides insight into both the inverse problem and the optimal survey design needed in azimuthally anisotropic media. Our analysis concentrates on P–wave reflection moveout in HTI media. Results of numerical applications and synthetic data examples show the accuracy and stability of the inversion procedure.

REFLECTION MOVEOUT IN HTI MEDIA

Al-Dajani and Tsvankin (1996) show that, for conventional spreadlengths and a horizontal reflector, reflection moveout for P–waves in homogeneous HTI media is sufficiently approximated by the conventional hyperbolic moveout equation. This equation is parameterized by the azimuthally dependent NMO velocity given in Tsvankin (1995). After recasting, his expression is

$$V_{\rm nmo}^2(\alpha) = \frac{V_{\rm s1}^2 V_{\rm s2}^2}{V_{\rm s1}^2 \sin^2\alpha + V_{\rm s2}^2 \cos^2\alpha}, \tag{1}$$

where $V_{\rm s1}$ and $V_{\rm s2}$ are the NMO velocity in the two vertical symmetry planes, and α is the angle between one of the symmetry planes and the survey line in 2D acquisition (or equivalently, source-to-receiver orientation in 3D acquisition). From equation (1), $V_{\rm s1}$ and $V_{\rm s2}$ are the semi-axes of what we call the NMO ellipse.

For pure P–wave propagation in HTI media, $V_{\rm s1} = V_{\rm Pvert}\sqrt{1+2\delta^{(\rm V)}}$ (NMO velocity in the symmetry-axis plane), $V_{\rm s2} = V_{\rm Pvert}$ (the vertical P–wave velocity), and α in this case is the angle between the symmetry-axis plane and the survey line direction. Here, $\delta^{(\rm V)}$ is Thomson's parameter δ for the equivalent VTI medium. For pure S–wave propagation, instead of the P–wave vertical velocity ($V_{\rm Pvert}$) we substitute the S–wave vertical velocities ($V_{\rm S\perp vert}$ for the slow shear wave and polarized normal to the cracks, and $V_{\rm S\parallel vert}$ for the fast shear wave and polarized parallel to the cracks) and instead of $\delta^{(\rm V)}$ we have $\sigma^{(\rm V)}$ and $\gamma^{(\rm V)}$ for the two shear-wave types, respectively; where $\sigma^{(V)} = (\frac{V_{\rm Pvert}}{V_{\rm S\perp vert}})^2(\epsilon^{(\rm V)} - \delta^{(\rm V)})$.

The elliptical variation of NMO-velocity with azimuth is well known for the case of an isotropic layer above a dipping interface (Levin, 1971). The NMO velocities in the dip and strike directions determine the semi-axes of the ellipse. Additionally, the

elliptical behavior of the NMO-velocity is a general phenomenon for arbitrarily dipping, layered azimuthally anisotropic media of any complexity (e.g., orthorhombic media) (Grechka and Tsvankin, 1996).

In HTI media, the effective NMO velocity for reflection from the bottom of layer N is well approximated, as shown by Al-Dajani and Tsvankin (1996), by the conventional Dix (1955) formula:

$$V_{\rm nmo}^2 = \frac{1}{t_0}\sum_{i}^{N} V_{2i}^2\,\Delta t_i\,, \tag{2}$$

where t_0 is the two-way zero-offset time to reflector N, V_{2i} is the interval NMO velocity for each individual layer i given by equation (1) for P-waves, and Δt_i is the two-way zero-offset time in layer i.

THE INVERSE PROBLEM

Because the azimuthal dependence of NMO velocity in an azimuthally anisotropic layer is elliptical [equation (1)], NMO velocities for three distinct survey-line azimuths are thus sufficient, as well as necessary, to reconstruct the elliptical distribution of the NMO velocity or, equivalently, to obtain the parameters $V_{\rm s1}$, $V_{\rm s2}$, and α. If the symmetry-plane directions are known, then NMO-velocity measurements in the two symmetry planes are sufficient to reconstruct the NMO velocity ellipse. Instead of inverting for the parameters of the ellipse [equation (1)], namely its orientation and the semi-axes, in HTI media we can estimate the medium parameters directly, simplifying the task of estimating crack density from P–wave reflection moveout.

In HTI media, for any number of input moveout velocity measurements, equation (1) yields two different sets of solutions for the two orthogonal symmetry axes, each with different combinations of $V_{\rm Pvert}$ and $\delta^{(\rm V)}$. One solution has a positive $\delta^{(\rm V)}$ with low $V_{\rm Pvert}$, while the other has a negative $\delta^{(\rm V)}$ with high $V_{\rm Pvert}$. Both solutions provide the same values of NMO velocity in all azimuthal directions; hence, we cannot distinguish between the symmetry-axis plane and isotropy plane from these measurements alone.

To illustrate this inverse problem, consider an HTI layer with $V_{\rm Pvert}$ = 2.0 km/s, $\delta^{(\rm V)}$ =-0.2, and the symmetry axis pointing in the x-axis direction (Figure 1a). Note that a $\delta^{(\rm V)}$ value of -0.2 approximately corresponds to a 20% azimuthal variation in the NMO velocity between the two symmetry-plane directions. Suppose we compute the NMO velocities along three different source-to-receiver azimuths (α_1, α_2, and α_3), measured from the symmetry-axis direction. As shown in Figure 1a, there are two sets of solutions corresponding to orthogonal directions of the symmetry axis that satisfy the three NMO velocities and produce the same elliptical variation of NMO velocity with azimuth (Figure 1b). Additional information, however, such as nonhyperbolic reflection moveout, with maximum magnitude in the symmetry-axis plane, can help to distinguish the symmetry-axis plane from the isotropy one and obtain the correct $V_{\rm Pvert}$ and $\delta^{(\rm V)}$. Furthermore, for typical ratios of the vertical velocities ($V_{S^\perp{\rm vert}}/V_{\rm Pvert} \leq .707$), the

parameter $\delta^{(V)}$ is negative (see Appendix A); therefore, the NMO velocity reaches its maximum in the isotropy plane and minimum in the symmetry-axis plane. Thus, if we assume that $\delta^{(V)} < 0$, we can identify unambiguously the symmetry-axis direction.

In 3-D (or, 2-D) land acquisition surveys or water-bottom cable surveys, we have relatively full control on offset and azimuthal coverage. Constructing a common-mid-point (CMP) gather for a specific azimuthal direction in 3-D acquisition survey, in general, requires collecting (sorting) traces from a range of azimuths (sectors). In conventional marine surveys, however, the azimuthal coverage is quite limited. Therefore, in order to obtain the required coverage along different azimuth directions the receiver lines (streamers) should be carried along those directions. Thus, multiple surveys will be necessary. Here, we investigate the choice of azimuth range for the azimuthal directions that provide best inversion results.

Intuitively, a maximum azimuthal separation between the survey lines (or, equivalently, between the source-to-receiver azimuths) can be expected to increase both stability and resolution; hence, setting the three azimuths 60° apart is of particular interest in our investigation. Moreover, some think in-line and cross-line directions provide the best offset coverage. We set two azimuths perpendicular to each other in the investigation in order to simulate this acquisition design.

ERROR ANALYSIS

To estimate the sensitivity of the NMO velocity to the anisotropic parameters, we evaluate the Jacobian of equation (1). The Jacobian is obtained by calculating the derivatives of NMO velocity with respect to the model parameters V_{Pvert}, $\delta^{(V)}$, and α. Although the NMO-velocity in equation (1) is nonlinear, its dependence on the anisotropy parameters is smooth enough to use the Jacobian for developing insight into the inverse problem. The derivatives used to form the Jacobian are as follows:

$$d_1(\alpha) = \frac{V_{\mathrm{Pvert}}}{V_{\mathrm{nmo}}(\alpha)} \frac{\partial V_{\mathrm{nmo}}(\alpha)}{\partial V_{\mathrm{Pvert}}} = 1,$$

$$d_2(\alpha) = \frac{1}{V_{\mathrm{nmo}}(\alpha)} \frac{\partial V_{\mathrm{nmo}}(\alpha)}{\partial \delta^{(V)}} = \frac{\cos^2 \alpha}{(1 + 2\delta^{(V)})[1 + 2\delta^{(V)} \sin^2 \alpha]},$$

$$d_3(\alpha) = \frac{1}{V_{\mathrm{nmo}}(\alpha)} \frac{\partial V_{\mathrm{nmo}}(\alpha)}{\partial \alpha} = -\frac{2\delta^{(V)} \sin \alpha \cos \alpha}{1 + 2\delta^{(V)} \sin^2 \alpha}.$$

The normalization of the derivatives chosen here simplifies the comparison of of each parameter's contribution to the NMO velocity. As a result, the information provided by these derivatives consists of relative values for V_{Pvert}, and absolute values for $\delta^{(V)}$ and α (the latter measured in radians).

The sensitivity of this inversion to errors in the input data (NMO velocities) can be estimated using the Jacobian matrix

$$J = \begin{pmatrix} d_1(\alpha_1) & d_2(\alpha_1) & d_3(\alpha_1) \\ d_1(\alpha_2) & d_2(\alpha_2) & d_3(\alpha_2) \\ d_1(\alpha_3) & d_2(\alpha_3) & d_3(\alpha_3) \end{pmatrix},$$

where α_1, α_2, and α_3 are the azimuths of the CMP gathers relative to the symmetry axis of the HTI model.

The condition number for the Jacobian matrix provides an approximate overall estimate of the quality (stability) of the inversion for all three parameters. In this paper, we will use the condition number as a criterion to design the best experimental setup. Then, we quantify propagation of errors to the medium parameters for a given error in the input measurements (NMO velocity) via a study of the covariance matrix and analysis of the numerical error.

Conditioning of the Problem

The reciprocal of the condition number, κ^{-1}, for the Jacobian matrix J is given by

$$\kappa^{-1} = \sqrt{\frac{|\lambda_{\min}|}{|\lambda_{\max}|}}, \tag{3}$$

where $\lambda_{\max}$ and $\lambda_{\min}$ are the maximum and minimum eigenvalues, respectively, of the matrix $A = J^T J$ (J^T is the transpose of J).

A small κ^{-1} number ($\approx$0) implies an ill-conditioned (i.e., nearly singular) problem, while a large κ^{-1} number usually implies a well-conditioned problem.

Figure 2 shows the reciprocal of the condition number, κ^{-1}, as a function of the middle azimuth α_2 and $\delta^{(V)}$, where the outer azimuths are $\alpha_1 = 0°$ and $\alpha_3 = 120°$. Notice that when the middle direction α_2 coincides with either of the two other azimuths (i.e., only two azimuths are available), the problem is clearly singular, with κ^{-1}=0. Note also that for $\delta^{(V)}$=0 (no azimuthal variation in NMO velocity, as in isotropic media), there is no symmetry-axis direction to resolve and again κ^{-1}=0. Since the ellipticity of the NMO-velocity function increases with increasing $|\delta^{(V)}|$, the stability improves with an increase in the absolute value of $\delta^{(V)}$. Not surprisingly, for typical values of $\delta^{(V)}$, as shown by Figure 2, the maximum of κ^{-1} (the highest stability) corresponds to the third-line direction α_2 being midway in between the two other lines. This is true for any angular separation. When the third azimuth orientation is close to any of the other two (intuitively a poor choice), the problem again becomes ill-conditioned. Figure 3 shows the results of this study for five different angular separations, $\Delta\alpha$, between the lines: (a) 7.5°, (b) 15°, (c) 30°, (d) 45°, and (e) 60°. κ^{-1} shows the least variation with azimuth for the maximum angular separation ($\Delta\alpha = 60°$) between the survey lines (curve *e* in Figure 3). Even though the global maximum for κ^{-1} is not associated with curve *e*, we should choose a survey design that has a higher overall stability for the whole range of azimuths, since we usually do not know the symmetry-axis direction in

advance. The angular separation of 45° (curve d in Figure 3), provides a higher value of κ^{-1} for a limited range of azimuths ($75° \leq \alpha_2 \leq 105°$) than that for the 60° angular separation; however, at other azimuths, κ^{-1} drops by about 50% (e.g., for $\alpha_2 = 30°$). This variation in κ^{-1} makes the 45° angular separation less desirable compared to the 60°. κ^{-1}; however, is not too small for any value of α_2 for curves d and e. Therefore, we should not expect any stability problem when those angular separations are used.

As expected, narrower angular separations ($< 45°$) do not provide stability comparable to that for 45° or 60°. Interestingly, curve c generates the global maximum for κ^{-1} for $\alpha_2 = 90°$. This local phenomenon, however, is particular for this case ($\delta^{(V)}$=-0.2) that appears neither in other azimuthal directions nor for smaller values of $\delta^{(V)}$ (Figure 4). For values other than $\alpha_2 = 90°$ the value of curve c's κ^{-1} is smaller than curve e's.

The same conclusions can be drawn for the model with weaker anisotropy (smaller $\delta^{(V)}$), shown in Figure 4. Notice that values for κ^{-1} in Figure 4 are smaller than those in Figure 3. Thus, κ^{-1} values are approximately linear to $\delta^{(V)}$.

Overall, the condition-number analysis shows that the widest angular separation between the azimuths (i.e., $\Delta\alpha = 60°$), provides a well-conditioned (well-behaved) inverse problem for any orientation of the three lines with respect to the symmetry axis.

Error Propagation (Covariance Matrix)

The propagation of errors from the input measurements (NMO velocity) to the medium parameters ($V_{\mathrm{Pvert}}, \delta^{(V)}$, and α) could be analyzed by calculating the covariance matrix of this inverse problem.

For the special case of a perfect forward modeling operator, a perfect parameterization of the model (i.e., no discretization errors), no *a priori* information, no uncertainties other than those associated with the input NMO-velocity data, and data uncertainties that are normally distributed with a known covariance, the covariance for the least-squares estimates of the model parameters is given by (Tarantola, 1987)

$$C_M = J^* C_D (J^*)^T , \tag{4}$$

where J^* is the pseudo-inverse of the Jacobian matrix, J of this inverse problem, and C_D is the data covariance matrix.

Let us further simplify the calculation by considering the fact that the Jacobian has the full-column rank [that is, three NMO velocity measurements along distinct source-to-receiver azimuths, for the range of angular separations that we are considering, do not produce zero eigenvalues (i.e., no null eigenvectors)] and that the data have independent, identically distributed errors with a known variance c_{d}. In this case, equation (4) reduces to

$$C_{\mathrm{m}} = c_{\mathrm{d}} [J^T J]^{-1} , \tag{5}$$

where c_{d} is a single measurement representing the variance of the input data (NMO velocity).

Thus, in the following analysis, we are estimating only the portion of the model covariance that comes from the forward modeling operator.

We will use the square-root of the diagonal elements of $C_{\rm m}$ to estimate the expected error (standard deviation) for each parameter: the absolute error in α measured in radians, the absolute error in $\delta^{(\rm V)}$, and the percentage error in $V_{\rm Pvert}$. If we set $c_{\rm d}$ to unity, the diagonal elements of $[J^T J]^{-1/2}$ simply measure the magnification factors of the error in each parameter for any given error in the input NMO-velocity measurements (given in percent). The magnification factors of the errors for the three parameters are denoted as M_α (measured in radians), $M_{\delta^{(\rm V)}}$ (dimensionless), and $M_{V_{\rm Pvert}}$ (dimensionless).

Similar to the analysis of the previous section, let us study the square-root of the covariance matrix (error propagation) as a function of the central azimuth, α_2, for three angular separations between the survey lines: $\Delta\alpha = 30°$, $45°$, and $60°$. The central azimuth, α_2, spans the angular range from $0°$ to $180°$ measured from the symmetry-axis direction. The variance of the input data (NMO-velocity) measurements $c_{\rm d}$ in equation (5), as described above, is set to unity. The resulting magnification factors for the errors in each parameter are shown in Figures 5-7.

As demonstrated by Figure 5, the accuracy in estimating the parameter α improves by a factor of about 3 by using an angular separation of $60°$, as opposed to $30°$, for most ranges of azimuths. For α_2 near the symmetry-plane directions, the error in α estimates, however, is about the same for the three angular separations. Where the symmetry-axis direction is not known in advance (as most often is the case), however, the behavior of the $30°$ angular separation is inappropriate. This indicates that the parameter α is quite sensitive to the set of azimuths used in the inversion procedure when $\Delta\alpha$ is small. For $\Delta\alpha = 45°$ we have similar observations, though to a lesser degree. The accuracy in estimating α is highest for an angular separation of $60°$ and is highly consistent for all orientations α_2. Notice again that the error in α varies inversely with the absolute value of $\delta^{(\rm V)}$ (Figure 5a compared to Figure 5b).

As shown in Figure 6, $\delta^{(\rm V)}$ is most stably estimated when $\Delta\alpha = 60°$. Note that the parameter $\delta^{(\rm V)}$ is also sensitive to the angular separation between the survey lines and the set of azimuths used in the inversion. Interestingly, the propagation of errors into $\delta^{(\rm V)}$ is about the same for different anisotropy strengths (compare Figure 6a with Figure 6b). This implies that we should expect the same absolute error in $\delta^{(\rm V)}$ for a wide range of $\delta^{(\rm V)}$, and the relative error in $\delta^{(\rm V)}$ will be smaller for stronger anisotropy.

Figure 7 demonstrates that the best accuracy in $V_{\rm Pvert}$ for all azimuths is again achieved for an angular separation of $60°$. The accuracy in resolving $V_{\rm Pvert}$ is about the same for the three angular separations when the central orientation α_2 is close to the isotropy-plane direction. Considering again the fact that the symmetry-axis direction is not known in advance, the choice of an angular separation of $30°$ (or any smaller angular separation) and, to some extent, $45°$ is inadequate. It is interesting to observe that the accuracy in estimating $V_{\rm Pvert}$ slightly increases as anisotropy becomes weaker (compare Figure 7b with Figure 7a). This is not surprising since $V_{\rm Pvert}$ is essentially an "isotropic" quantity, and it can be expected to be best resolved when the medium is

isotropic ($\delta^{(V)} = 0$).

To compute the expected absolute error (standard deviation) in the estimated symmetry-axis direction α for a particular angular separation between the survey lines, we

- Pick the magnification factor for a given set of azimuths from Figure 5.
- Multiply this factor by the error (standard deviation) in the input NMO-velocity measurements to get the absolute error in α (in radians).

Similarly, to estimate the absolute error in $\delta^{(V)}$, we apply the same procedure but using Figure 6. For V_{Pvert}, Figure 7 should be used to find the percentage error in this parameter. For example, consider an azimuth combination of $\alpha_1 = 0°$, $\alpha_2 = 60°$, and $\alpha_3 = 120°$ and a model with $V_{Pvert} = 2.0$ km/s and $\delta^{(V)} = -0.2$. From Figures 5a, 6a, and 7a, an error in the input NMO-velocity measurements of $\pm 1.6\%$ is expected to cause the following errors in the medium parameters: ± 0.048 radians in α ($\pm 2.75°$), ± 0.02 in $\delta^{(V)}$, and $\pm 2.2\%$ in V_{Pvert} (± 0.044 km/s).

It is important to mention that in the case of land seismic data acquisition, wide azimuthal data coverage (≥ 45) is quite feasible. In marine cases, however, the maximum azimuthal coverage is about 30°. As a demonstration, error propagation for the parameter α is simulated in Figure 8. Note the huge magnification of error in the case of narrow azimuthal separations. Therefore, in marine acquisition, in order to ensure that the estimated parameters contain minimum errors, we should have multiple azimuthal surveys (60° apart).

Overall, from Figures 5-8, we conclude that the best angular separation for the inversion procedure is 60°. All three parameters are sensitive to the angular separation between the survey lines. The sensitivity to the orientations of the survey lines is large for small $\Delta\alpha$, but small for $\Delta\alpha = 60°$. Unlike V_{Pvert} and $\delta^{(V)}$, the accuracy in estimating the parameter α, in particular, is quite sensitive to the strength of anisotropy (the errors in α estimates vary inversely with the strength of anisotropy).

Numerical Inversion

The above analysis based on the Jacobian matrix is approximate since the NMO-velocity equation (1) is nonlinear. In this section, we perform nonlinear inversion by means of the Newton-Raphson method and study the sensitivity of the results to errors in the input information. We consider the same HTI models studied earlier, with $\delta^{(V)} = -0.1$ and $\delta^{(V)} = -0.2$, both with $V_{Pvert} = 2.0$ km/s. After 100 trials with $\pm$ 3 % range of uniformly-distributed random errors (standard deviation of about 1.6 %) introduced into the exact NMO velocities, we obtain the results displayed in Table 1 for $\delta^{(V)} = -0.2$, and in Table 2 for $\delta^{(V)} = -0.1$. The different three source-to-receiver azimuths used to conduct these tests are displayed in Table 3. It is important to mention, as discussed earlier that for each trial two different sets of solutions are obtained that satisfy the input NMO velocities. The correct solution is selected under the assumption that the parameter $\delta^{(V)}$ is typically negative.

Supporting the conclusions of the error analysis, the inversion results in Tables 1 and 2 demonstrate that the azimuth of the symmetry-axis plane, the parameter α, is better estimated as the absolute value of $\delta^{(V)}$ increases (error reduction is almost linearly proportional to $\delta^{(V)}$). Comparing the inversion results for $\delta^{(V)}$ in Table 1 with their counterparts in Table 2, we observe that the improvement in the estimation is not significant with increase in $\delta^{(V)}$. Also, the errors in estimating V_{Pvert} are somewhat smaller in the case of weaker anisotropy (e.g., compare set 9 in both Tables 1 and 2).

Consistent with the covariance study, the smallest errors, measured by the mean and the standard deviation, are associated with sets of azimuths with maximum separation between the survey lines ($\Delta\alpha = 60°$), especially for the symmetry-axis direction α (sets 9-12 in Tables 1 and sets 9-10 in Table 2). An angular separation of 45° provides an accuracy (e.g., sets 5-8) comparable to the one for the 60° separation, especially for $\delta^{(V)}$ and V_{Pvert}. Note that the accuracy for α deteriorates when two of the selected azimuths happen to coincide with the symmetry planes of the medium (set 5 as opposed to set 7). As expected, the worst results correspond to narrow azimuthal separations (sets 1 and 2).

The variations in the mean and the size of standard deviation of the three parameters in Tables 1 and 2 are thus consistent with the results of the covariance-matrix analysis. It should be mentioned, however, that having more than three distinct source-to-receiver azimuths (e.g., full azimuthal coverage) provides a useful data redundancy. This redundancy enhances the quality of the estimates and sets the stage for a least-square type of inversion in which the errors in the parameters estimates are minimized in a least-square sense. Actually, with N number of observations (solutions), the error bars (standard deviation) will reduce by a factor of $1/\sqrt{N-1}$.

	-	Set 1	-	-	Set 2	-	-	Set 3	-
	V_{Pvert}	$\delta^{(\mathrm{V})}$	α	V_{Pvert}	$\delta^{(\mathrm{V})}$	α	V_{Pvert}	$\delta^{(\mathrm{V})}$	α
mean	2.24	-0.23	19.5	2.04	-0.21	0.9	2.0	-0.2	60.1
std dev	0.87	0.11	29.5	0.14	0.03	9.1	0.03	0.02	3.1
	-	Set 4	-	-	Set 5	-	-	Set 6	-
	V_{Pvert}	$\delta^{(\mathrm{V})}$	α	V_{Pvert}	$\delta^{(\mathrm{V})}$	α	V_{Pvert}	$\delta^{(\mathrm{V})}$	α
mean	2.0	-0.20	0.8	2.01	-0.20	0.5	2.0	-0.20	29.9
std dev	0.05	0.02	6.1	0.03	0.01	4.8	0.03	0.02	3.2
	-	Set 7	-	-	Set 8	-	-	Set 9	-
	V_{Pvert}	$\delta^{(\mathrm{V})}$	α	V_{Pvert}	$\delta^{(\mathrm{V})}$	α	V_{Pvert}	$\delta^{(\mathrm{V})}$	α
mean	2.0	-0.20	45.3	2.0	-0.20	-44.87	2.0	-0.20	0.4
std dev	0.03	0.02	2.8	0.08	0.03	2.9	0.04	0.02	2.8
	-	Set 10	-	-	Set 11	-	-	Set 12	-
	V_{Pvert}	$\delta^{(\mathrm{V})}$	α	V_{Pvert}	$\delta^{(\mathrm{V})}$	α	V_{Pvert}	$\delta^{(\mathrm{V})}$	α
mean	1.99	-0.20	31.0	2.0	-0.20	-60.3	2.0	-0.20	45.4
std dev	0.03	0.01	3.5	0.04	0.02	3.0	0.04	0.02	3.4

Table 1: Inversion results using the twelve different sets of source-to-receiver azimuths given in Table 3. Here, $\delta^{(\mathrm{V})}$ = -0.2 and V_{Pvert} = 2.0 km/s.

	-	Set 5	-	-	Set 7	-
	V_{Pvert}	$\delta^{(\mathrm{V})}$	α	V_{Pvert}	$\delta^{(\mathrm{V})}$	α
mean	2.01	-0.11	0.5	2.0	-0.10	43.4
std dev	0.03	0.02	10.1	0.03	0.03	8.2
	-	Set 9	-	-	Set 10	-
	V_{Pvert}	$\delta^{(\mathrm{V})}$	α	V_{Pvert}	$\delta^{(\mathrm{V})}$	α
mean	2.01	-0.11	1.0	2.0	-0.10	29.9
std dev	0.03	0.02	7.2	0.03	0.02	7.5

Table 2: Inversion results using four different sets of source-to-receiver azimuths given in Table 3. Here, $\delta^{(\mathrm{V})}$ = -0.1 and V_{Pvert} = 2.0 km/s.

Set	-	Azimuths	-
1	0°	15°	30°
2	0°	30°	60°
3	60°	105°	150°
4	0°	75°	150°
5	0°	45°	90°
6	30°	75°	120°
7	45°	90°	135°
8	−45°	0°	45°
9	0°	60°	120°
10	30°	90°	150°
11	−60°	0°	60°
12	45°	105°	165°

Table 3: Sets of azimuth combinations used to generate the numerical results in Tables 1 and 2. The source-to-receiver azimuths are measured from the symmetry-axis direction. An azimuth direction of 150° is the same as −30°.

THE INVERSE PROBLEM IN LAYERED MEDIA

So far we have considered the inverse problem for a single homogeneous HTI layer. However, a fractured zone characterized by the HTI symmetry may be overlain by an inhomogeneous and anisotropic overburden. In this section, the inverse problem is studied for a model with an azimuthally isotropic overburden (e.g., purely isotropic, VTI, or both) above the HTI layer. Once the interval NMO velocities in the HTI layer have been found by conventional Dix differentiation (layer-stripping) of the moveout velocity from the top and bottom of the HTI layer, we can apply the single-layer inversion discussed above. An additional question to be addressed, however, is how the relative thickness of the HTI layer (compared with the total thickness) influences on the stability and accuracy of the parameter estimation. Before discussing this inverse problem and addressing this issue, let us consider a synthetic (noise-free) model.

Consider a model common for fractured reservoirs, which contains five homogeneous isotropic layers overlaying an HTI layer, as shown in Figure 9. Using a 3-D anisotropic ray-tracing code developed by Gajewski and Pšenčik (1987), the exact traveltime reflections were generated as a function of offset along five source-to-receiver lines: 0°, 30°, 45°, 60°, and 90° (Figure 9). The traveltime-offset curves are plotted in Figure 10. Conventionally, stacking velocity is estimated using semblance (coherency) analysis. Here, however, NMO velocity is estimated by fitting a hyperbola to the traveltime curve in a least-squares sense. Thus, NMO (stacking) velocity is obtained:

$$V^2_{\rm nmo} = \frac{\sum_{j=1}^{N} x_j^2}{\sum_{j=1}^{N} t_j^2 - N\, t_0^2},$$

where x_j is the offset of the j-th trace, t_j is the corresponding two-way reflection traveltime, t_0 is the two-way vertical traveltime, and N is the number of traces. A spread-length of 1.5 km is used to compute the NMO velocity. In the least-squares fitting procedure, the vertical time t_0 was fixed at the correct value.

Applying Dix differentiation for the NMO velocity from the top and bottom of the HTI layer, we obtain an estimate of the interval $V_{\rm nmo}$ as a function of azimuth (Figure 11). Even though estimating the NMO velocity on finite spreads, in general, introduces errors due to the influence of nonhyperbolic moveout and due to the fact that Dix differentiation outside the symmetry planes is approximate (Al-Dajani and Tsvankin, 1996), we obtain relatively accurate values for the interval NMO velocity for all azimuths (Figure 11). It is important to mention that as seen in Figure 11, the difference between the estimated and the exact interval NMO velocities is due to the combined influence of nonhyperbolic moveout and dix differentiation. Since $\delta^{(V)} < 0$, the maximum interval NMO velocity in Figure 11 corresponds to the fracture orientation (isotropy plane), while the minimum is observed in the symmetry-axis direction. If $\delta^{(V)} > 0$ (which is not likely in HTI media, see Appendix A), the minimum interval NMO velocity would correspond to the isotropy plane.

From equation (1), the interval $\delta^{(V)}$ can be obtained from the interval NMO velocities in the two symmetry planes as

$$\delta^{(V)} = \frac{1}{2}\left(\frac{V_{\rm nmo_{min}}}{V_{\rm nmo_{max}}}\right)^2 - \frac{1}{2}, \tag{6}$$

where $V_{\rm nmo_{min}}$ and $V_{\rm nmo_{max}}$ are the estimated interval NMO velocities along the symmetry-axis direction and in the isotropy plane, respectively, and $\delta^{(V)}$ is assumed to be negative.

The estimated $\delta^{(V)}$ for the HTI layer using equation (6) and the interval NMO velocities in Figure 11 is -0.312 where the correct value is -0.318.

In the following section, we conduct an error analysis for this inverse problem to quantify issues such as accuracy, stability, and error propagation for HTI media.

Error Analysis

To set up the inverse problem, consider the model shown in Figure 12, where the NMO velocity for reflections from the bottom of the HTI layer is given by the Dix equation:

$$V_{\rm N}^2 = V_{\rm N-1}^2(1-\rho) + V_{\rm nmo}^2\rho\,, \tag{7}$$

with $V_{\rm N-1}$ being the NMO velocity for a reflection from the top of the HTI layer, $V_{\rm nmo}$ is the interval NMO velocity of the HTI layer given by equation (1), and $\rho = \Delta t_{\rm N}/T_{\rm N}$ is the ratio of the two-way interval traveltime $\Delta t_{\rm N}$ in the HTI layer to the two-way total traveltime $T_{\rm N}$ from the surface to the bottom of the HTI layer.

From equation (7), the interval NMO velocity for the HTI layer can be represented as

$$V_{\rm nmo}^2 = \frac{V_{\rm N}^2 - V_{\rm N-1}^2(1-\rho)}{\rho}\,. \tag{8}$$

Therefore, the interval NMO velocity in the HTI layer estimated in the inversion process is dependent on the relative thickness of the layer ρ. This fact, which is well known from isotropic interval velocity analysis, influences the accuracy of the parameter estimation in the HTI layer. In order to gain more insight into this inverse problem, we conduct the following error analysis.

To study the sensitivity of the effective NMO velocity to the anisotropic parameters of the HTI layer and the layer thickness, we evaluate the Jacobian of equation (7). The derivatives used to form the Jacobian are

$$d_1(\alpha) = \frac{V_{\mathrm{N}-1}}{V_{\mathrm{N}}(\alpha)} \frac{\partial V_{\mathrm{N}}(\alpha)}{\partial V_{\mathrm{N}-1}},$$

$$d_2(\alpha) = \frac{V_{\mathrm{Pvert}}}{V_{\mathrm{N}}(\alpha)} \frac{\partial V_{\mathrm{N}}(\alpha)}{\partial V_{\mathrm{Pvert}}},$$

$$d_3(\alpha) = \frac{1}{V_{\mathrm{N}}(\alpha)} \frac{\partial V_{\mathrm{N}}(\alpha)}{\partial \delta^{(\mathrm{V})}},$$

and

$$d_4(\alpha) = \frac{1}{V_{\mathrm{N}}(\alpha)} \frac{\partial V_{\mathrm{N}}(\alpha)}{\partial \alpha}.$$

Again, the normalization of the derivatives simplifies the assessment of the relative importance of each parameter. Hence, the information provided by these derivatives consists of relative values for $V_{\mathrm{N}-1}$, and V_{Pvert}, and absolute values for $\delta^{(\mathrm{V})}$ and α (measured in radians within the layer). Note that $V_{\mathrm{N}-1}$ is not an unknown (it is one of our measurements), but it is included in the Jacobian to simplify the analysis of the inverse problem.

The sensitivity of this inversion to errors in the input data (i.e., NMO velocity at the top and bottom of the HTI layer) can be assessed from the Jacobian matrix

$$J = \begin{pmatrix} 1 & 0 & 0 & 0 \\ d_1(\alpha_1) & d_2(\alpha_1) & d_3(\alpha_1) & d_4(\alpha_1) \\ d_1(\alpha_2) & d_2(\alpha_2) & d_3(\alpha_2) & d_4(\alpha_2) \\ d_1(\alpha_3) & d_2(\alpha_3) & d_3(\alpha_3) & d_4(\alpha_3) \end{pmatrix},$$

where α_1, α_2, and α_3 are the azimuths of the CMP gathers measured from the symmetry-axis of the HTI layer.

As shown above, to obtain maximum stability and accuracy, the best set of azimuths for use in the inversion process corresponds to the maximum angular separation, $\Delta\alpha = 60°$. This conclusion remains valid here as well. Hence, in the upcoming tests we set the azimuths to $\alpha_1 = 0°, \alpha_2 = 60°$, and $\alpha_3 = 120°$ to concentrate on the dependence of the inversion results on ρ and $\delta^{(\mathrm{V})}$.

The stability of the inverse problem for this azimuthal separation, measured using the reciprocal of the condition number [equation (3)], is linearly proportional to the

layer thickness ratio (ρ) for $\rho < 0.4$ (Figure 13). For $\rho > 0.4$, κ^{-1} flattens out, as seen in Figure 13. Also, as in the homogeneous case, the stability increases (approximately linearly) with an increase in the absolute value of $\delta^{(V)}$ (compare Figure 13a with Figure 13b). As we expect, for small thickness ratios (e.g., $\rho < 0.1$) the inverse problem is ill-conditioned.

To study the propagation of error (standard deviation) into the parameters of the HTI layer as a function of the thickness ratio ρ for a given error in the input measurements (NMO velocity for reflections from the top and bottom of the HTI layer), we compute the covariance matrix [equation (5)] for the Jacobian matrix J of this inverse problem. The assumptions here are the same as those for the homogeneous case discussed earlier. Setting the variance of the input NMO-velocity measurements to unity means that the square-root of the covariance represents the magnification of error (standard deviation) in each parameter for any given error (standard deviation) in the input NMO-velocity. Figure 14 shows the error magnification factors (the square-root of the diagonal elements of $[J^T J]^{-1/2}$) as a function of ρ: (a) magnification factor in the absolute error in α (M_α) measured in radians, (b) magnification factor in the absolute error in $\delta^{(V)}$ ($M_{\delta(V)}$), and (c) magnification factor in the percentage error in V_{Pvert} ($M_{V_{Pvert}}$). As seen in Figure 14, the magnification of error in each parameter is proportional to $1/\rho$. Thus, for $\rho < 0.4$ the resolution, measured by the square-root of the variance (i.e., standard deviation), improves significantly (linearly) as ρ increases. For $\rho > 0.4$ the resolution remains almost the same, which is consistent with the results obtained from the reciprocal of the condition number.

Numerical Inversion in Layered Media

In this section we perform the nonlinear inversion of NMO velocity in layered media by means of the Newton-Raphson method (as for the single-layer model) and study the sensitivity of the results to errors in the input information (NMO velocity at the top and bottom of the HTI layer) as a function of ρ. Consider two HTI models, with $\delta^{(V)} = -0.1$ and $\delta^{(V)} = -0.2$, both of which have $V_{Pvert} = 3.0$ km/s, and the NMO velocity at the top of the HTI layer, $V_{N-1} = 2.0$ km/s. From the study of the single-layer model, azimuthal separation of 60° between the survey azimuths, in general, produces the best inversion results. Let us select here $\alpha_1 = 0°, \alpha_2 = 60°$, and $\alpha_3 = 120°$ to be the three source-to-receiver azimuths used in the inversion process. From 100 trials with $\pm$ 3 % range of random error introduced to the exact NMO velocities at the top and bottom of the HTI layer, we obtain the perturbed interval NMO velocities (using Dix differentiation), which are then used to estimate the parameters of the HTI layer. The solutions (the mean and standard deviation) as a function of ρ are displayed in Figure 15 for $\delta^{(V)} = -0.2$ (a, b, and c) and for $\delta^{(V)} = -0.1$ (d, e, and f). As in the homogeneous case, the solutions are obtained under the assumption that the parameter $\delta^{(V)}$ is negative.

Consistent with the study of the covariance matrix, Figure 15 shows that the errors in the estimates do not change much for $\rho > 0.4$, and vary significantly (almost inversely)

with ρ for small ρ. That is, for small thickness ratios ($\rho < 0.4$), the error in the parameter estimation is magnified by the factor $1/\rho$ compared to the error in the effective NMO velocity, as expected from equation (8).

The parameter α is better resolved for higher absolute value of $\delta^{(V)}$ (Figures 15a and 15d) (e.g., the error bars for α become twice as large when $\delta^{(V)}$ changes from -0.2 to -0.1). The improvement in the accuracy in estimating the parameter $\delta^{(V)}$ with increasing $\delta^{(V)}$ is not as dramatic as that in α (Figures 15b and e). As in the single-layer model, the absolute error measured by the error bars is almost the same for both values of $\delta^{(V)}$; therefore, the relative error is smaller for stronger anisotropy. The accuracy of V_{Pvert} estimates, as in the single-layer case, slightly improves for weaker anisotropy (Figures 15c and f).

As demonstrated by Figure 15, an HTI layer overlain by an azimuthally isotropic overburden should have a relative thickness (in time) to the total thickness of at least equal to the ratio of the error in the NMO (stacking) velocity to the interval anisotropy strength of the fractured layer. For example, for typical errors in the estimated NMO (stacking) velocity ($\leq 2\%$), as is the case in this numerical study, the minimum ratio of thickness (in time) of the HTI layer to the total thickness, ρ, needed to resolve the three parameters with acceptable accuracy when $\delta^{(V)} = -0.1$ is at least about 0.2 [Figures (15d-f)]. As the strength of anisotropy in the HTI layer increases ($\delta^{(V)} = -0.2$), we obtain acceptable medium parameter estimates for smaller values of ρ [e.g., 0.1 in Figures (15a-c)]. It is important to mention, however, that parameter estimation may become unstable for an HTI layer with weak azimuthal anisotropy ($|\delta^{(V)}| < 0.1$, which corresponds to azimuthal interval-NMO-velocity variation $< 10\%$), especially for small values of ρ ($\rho < 0.2$). The significant deviation of the mean from the true solution in Figure (15b, c, e, and f) for $\rho < 0.2$ can be interpreted as a direct indication of instability in the inversion process. Larger errors in the NMO-velocity estimates ($> 2\%$) cause the required minimum relative thickness of the HTI layer to be larger in order to obtain acceptable inversion results.

It is important to emphasize that, as we have seen in the previous sections, three NMO velocity measurements along three distinct survey lines in 2-D cases or, equivalently, azimuth orientations in 3-D acquisition with angular separation of 60°, are best for performing the inversion procedure. Coverage along other directions, however, adds some redundancy which may become useful in enhancing the quality of the inversion process.

DISCUSSION AND CONCLUSIONS

We have discussed reflection moveout inversion for azimuthally anisotropic media, with emphasis on P-wave reflection moveout for horizontal transverse isotropy (HTI). NMO-velocity measurements obtained for three distinct survey azimuths are sufficient to invert for the three medium parameters (V_{Pvert}, $\delta^{(V)}$, and α), under the assumption that $\delta^{(V)}$ is typically negative. Without this assumption, additional information, such as the

azimuthal variation in nonhyperbolic moveout, is needed to distinguish between the symmetry-axis and the isotropy planes. For HTI models with parallel penny-shaped cracks, the symmetry axis is normal to the crack plane. Hence, the azimuthal dependence of reflection moveout in HTI media makes it possible to detect the crack orientation.

Parameter estimation from variations in the moveout velocity in HTI media is quite sensitive to the angular separation between the survey lines and to the set of azimuths used in the inversion procedure. The accuracy in estimating the orientation of the symmetry planes, α, in particular, is also sensitive to the strength of anisotropy, with error inversely proportional to the strength of anisotropy. In order to maximize the accuracy and stability in parameter estimation, it is best to have the azimuths for the three source-to-receiver directions 60° apart. The accuracy in resolving the parameters for an angular separation of 60° is consistent at all azimuths, and for most ranges of azimuths the associated errors are the least.

In HTI media, the accuracy in resolving $\delta^{(V)}$ is about the same for any strength of anisotropy, with a slight improvement with increasing $|\delta^{(V)}|$. Similarly, the accuracy in estimating $V_{P\text{vert}}$ is about the same for any strength of anisotropy, with a slight improvement as anisotropy becomes weaker.

Three NMO velocity measurements along three distinct survey lines in 2-D cases or, equivalently, azimuth orientations in 3-D acquisition with angular separation of 60°, are best for performing the inversion procedure.

In 3-D land and ocean-bottom-cable acquisition, where the acquisition is relatively flexible, it is recommended to have azimuthal coverage along at least three directions, 60° apart. In conventional marine (streamer) surveys, the azimuthal coverage is quite limited. Therefore, in order to obtain the required coverage along the optimal azimuth directions (60° apart), the receiver lines (streamers) should be carried along those directions, which means multiple surveys are needed.

In general, having more than three distinct source-to-receiver azimuths (e.g., full azimuthal coverage) provides a useful data redundancy that enhances the quality of the estimates, and sets the stage for a least-square type of inversion in which the errors in the parameters estimates are minimized in a least-square sense. Actually, with N number of observations (solutions), the error bars (standard deviation) will reduce by a factor of $1/\sqrt{N-1}$.

If the orientation of the symmetry axis is known, then two NMO-velocity measurements (two survey azimuths) are sufficient to invert for $V_{P\text{vert}}$ and $\delta^{(V)}$. Since normal-moveout velocity has a nonlinear dependence on the azimuthal angle α ($\sin^2\alpha$), at least two NMO velocity observations are necessary to identify the orientation of the symmetry-axis using known values of $V_{P\text{vert}}$ and $\delta^{(V)}$.

An HTI layer overlain by an azimuthally isotropic overburden (as might happen for fractured reservoirs) should have a relative thickness (in time) to the total thickness. The total thickness should be at least equal to the ratio of the error in the NMO (stacking) velocity to the interval anisotropy strength of the fractured layer. For example, a relative

thickness (in time) with respect to the total thickness of at least 0.2 is needed in order to obtain acceptable estimates of the medium parameters, provided that the azimuthal variation in the interval NMO velocity within the azimuthally anisotropic layer is about 10% and the error in the input NMO velocity measurement is 2%.

The conclusions made here for P–wave reflection moveout inversion in HTI media, such as the appropriate set of azimuths to be used for the inversion and the minimum thickness of the layer required for reliable estimates for the medium parameters, are also valid for pure S–wave propagation. In this case, however, instead of the P–wave vertical velocity (V_{Pvert}) we have the S–wave vertical velocities ($V_{\mathrm{S}\perp\mathrm{vert}}$ and $V_{\mathrm{S}\parallel\mathrm{vert}}$) and instead of $\delta^{(\mathrm{V})}$ we have $\sigma^{(\mathrm{V})}$ and $\gamma^{(\mathrm{V})}$ for the two shear-wave types, respectively. Even though the emphasis of our discussion is on HTI media, the NMO velocity variation with azimuth is similar (elliptical) for more complicated azimuthally anisotropic media. The key difference is the interpretation of the semi-axes of the NMO-ellipse [equation (1)]. A generalization of the presented conclusions to arbitrary azimuthally anisotropic media will be addressed in a future paper.

Finally, it would be advantageous to integrate this methodology with other seismic exploration techniques, such as azimuthal amplitude-variation-with-offset analysis and borehole information, to reduce the ambiguity in the estimation of the medium parameters.

ACKNOWLEDGMENTS

We would like to thank the Earth Resources Laboratory (ERL) at the Massachusetts Institute of Technology (MIT), and the Stanford Exploration Project (SEP) at Stanford University for technical support. We are grateful to Professors Nafi Toksöz and Dale Morgan (MIT), and Ken Larner and Ilya Tsvankin (Colorado School of Mines) for useful critiques. Al-Dajani would like to thank the Saudi Arabian Oil Company (Saudi Aramco) for financial support. This work was also supported by the Borehole Acoustics and Logging/Reservoir Delineation Consortia at M.I.T.

REFERENCES

Al-Dajani, A. and Tsvankin, I., 1996, Nonhyperbolic reflection moveout for horizontal transverse isotropy, *Geophysics,* in press (also in the *66th SEG Expanded Abstracts*).

Crampin, S., McGonigle, R., and Bamford, D., 1980, Estimating crack parameters from observations of P-wave velocity anisotropy, *Geophysics, 5*, 345–360.

Dix, C.H., 1955, Seismic velocities from surface measurements, *Geophysics, 20*, 68–86.

Gajewski, D., and Pšenčik, I., 1987, Computation of high-frequency seismic wavefields in 3-D laterally inhomogeneous anisotropic media, *Geophys. J. R. Astr. Soc., 91*, 383–411.

Grechka, A. and Tsvankin, I., 1996, 3-D description of normal moveout in anisotropic media, *66th Ann. Internat. Mtg., Soc. Expl. Geophys., Expanded Abstracts,* 1487–1490.

Levin, F.K., 1971, Apparent velocity from dipping interface reflections, *Geophysics, 36*, 510–516.

Lynn, H.B., Bates, C.R., Simon, K.M., Van Doc, R., 1995, The effects of azimuthal anisotropy in *P*-wave 3-D seismic, *65th Ann. Internat. Mtg., Soc. Expl. Geophys., Expanded Abstracts,* 727–730.

Mallick, S., Craft, K.L., Meister, L.J., and Chambers, R.E., 1996, Determination of the principal directions of azimuthal anisotropy from *P*-wave seismic data, *58th EAGE Expanded Abstracts.*

Rüger, A., 1995, *P*-wave reflection coefficients for transversely isotropic media with vertical and horizontal axis of symmetry, *65th Annual Internat. Mtg., Soc. Expl. Geophys., Expanded Abstracts,* 278–281.

Sena, A.G., 1991, Seismic traveltime equations for azimuthally anisotropic and isotropic media: Estimation of internal elastic properties, *Geophysics, 56*, 2090–2101.

Tarantola, A., 1987, *Inverse Problem Theory*, New York, Elsevier.

Thomsen, L., 1986, Weak elastic anisotropy, *Geophysics, 51*, 1954–1966.

Thomsen, L., 1988, Reflection seismology over azimuthally anisotropic media, *Geophysics, 53*, 304–313.

Thomsen, L., 1995, Elastic anisotropy due to aligned cracks in porous rock, *Geophysical Prospecting, 43*, 805–830.

Tsvankin, I., 1995, Inversion of moveout velocities for horizontal transverse isotropy, *65th Annual Internat. Mtg., Soc. Expl. Geophys., Expanded Abstracts,* 735–738.

Tsvankin, I., 1997, Anisotropic parameters and P-wave velocity for orthorhombic media, *Geophysics, 62*, 1292–1309.

APPENDIX

SIGN OF HTI PARAMETERS

In order to determine the sign of $\delta^{(V)}$ in HTI media due to parallel cracks, we use the shear wave splitting parameter γ given in Tsvankin (1995) as a function of the HTI parameters:

$$\gamma = \frac{V^2_{P\text{vert}}}{2\,V^2_{S^\perp\text{vert}}}\left[\frac{\epsilon^{(V)}\,[2-1/f^{(V)}]-\delta^{(V)}}{1+2\epsilon^{(V)}/f^{(V)}+\sqrt{1+2\,\delta^{(V)}/f^{(V)}}}\right].$$

The shear wave splitting parameter γ is a positive quantity (Thomsen, 1988). Since the denominator of the term between brackets is also a positive quantity, as well as the ratio of the vertical velocities, we obtain

$$\epsilon^{(V)}\,[2-1/f^{(V)}]-\delta^{(V)} = C\gamma\,,$$

where $C\gamma$ is a positive quantity.

Therefore,

$$\epsilon^{(V)}\,[2-1/f^{(V)}]-\delta^{(V)} - C\gamma = 0\,.$$

Hence,

$$\delta^{(V)} = \epsilon^{(V)}\,[2-1/f^{(V)}] - C\gamma\,.$$

Substituting $\epsilon^{(V)}$ in terms of the generic coefficient ϵ (defined relative to the horizontal symmetry axis, see Tsvankin, 1995, or Rüger, 1995) gives

$$\delta^{(V)} = \frac{\epsilon}{1+2\epsilon}[1/f^{(V)}-2] - C\gamma\,.$$

Since $\epsilon \geq 0$ for a single system of cracks and $C\gamma$ is also a positive quantity, the sign of $\delta^{(V)}$ depends on the sign of the term

$$1/f^{(V)} - 2 = 2\left(\frac{V_{S^\perp\text{vert}}}{V_{P\text{vert}}}\right)^2 - 1\,,$$

Therefore, if $\frac{V_{S^\perp\text{vert}}}{V_{P\text{vert}}} \leq 0.707$, $\delta^{(V)}$ is always negative. Even if $\frac{V_{S^\perp\text{vert}}}{V_{P\text{vert}}} \geq 0.707$, $\delta^{(V)}$ can still be negative depending on the term $C\gamma$.

For pure S-wave propagation (the fast shear wave $S^{\|}$ and the slow shear wave $S^{\perp}$), the NMO-velocity functions are governed by the anisotropy parameters $\gamma^{(V)}$ and $\sigma^{(V)}$ for the two shear-wave types, respectively; where $\sigma^{(V)} = (\frac{V_{P\text{vert}}}{V_{S^\perp\text{vert}}})^2(\epsilon^{(V)} - \delta^{(V)})$.

The parameter $\gamma^{(V)}$ defined in terms of the generic coefficient γ (defined relative to the horizontal symmetry axis, see Tsvankin, 1995, or Rüger, 1995) is given as

$$\gamma^{(V)} = -\frac{\gamma}{1+2\gamma}$$

and γ is a positive quantity. Therefore, $\gamma^{(V)}$ is always negative.

The sign of the parameter $\sigma^{(V)}$, on the other hand, is not as obvious as that for the other parameters. It depends solely on the sign of the combination $(\epsilon^{(V)} - \delta^{(V)})$. Both $\epsilon^{(V)}$ and $\delta^{(V)}$ are negative quantities, but the difference between the two is typically a positive quantity. There is nothing, however, to prevent $\sigma^{(V)}$ from being a negative quantity.

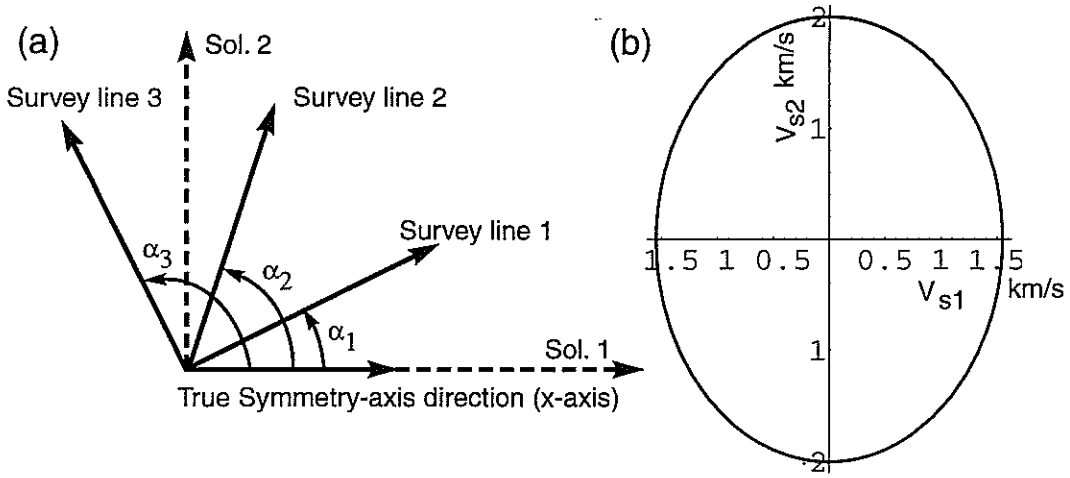

Figure 1: (a) Plan view of three 2D survey lines (source-to-receiver azimuths in 3D) over a horizontal HTI layer with $V_{\mathrm{Pvert}} = 2.0$ km/s, and $\delta^{(\mathrm{V})} = -0.2$, with the symmetry-axis in the x direction. Two different sets of solutions for the symmetry-axis direction (dashed lines) provide the same NMO-velocity variation, as shown in (b). The correct solution (Sol. 1, horizontal dashed line) has $V_{\mathrm{Pvert}} = 2.0$ km/s and $\delta^{(\mathrm{V})} = -0.2$, while Sol. 2 has $V_{\mathrm{Pvert}} = 1.549$ km/s and $\delta^{(\mathrm{V})} = 0.333$.

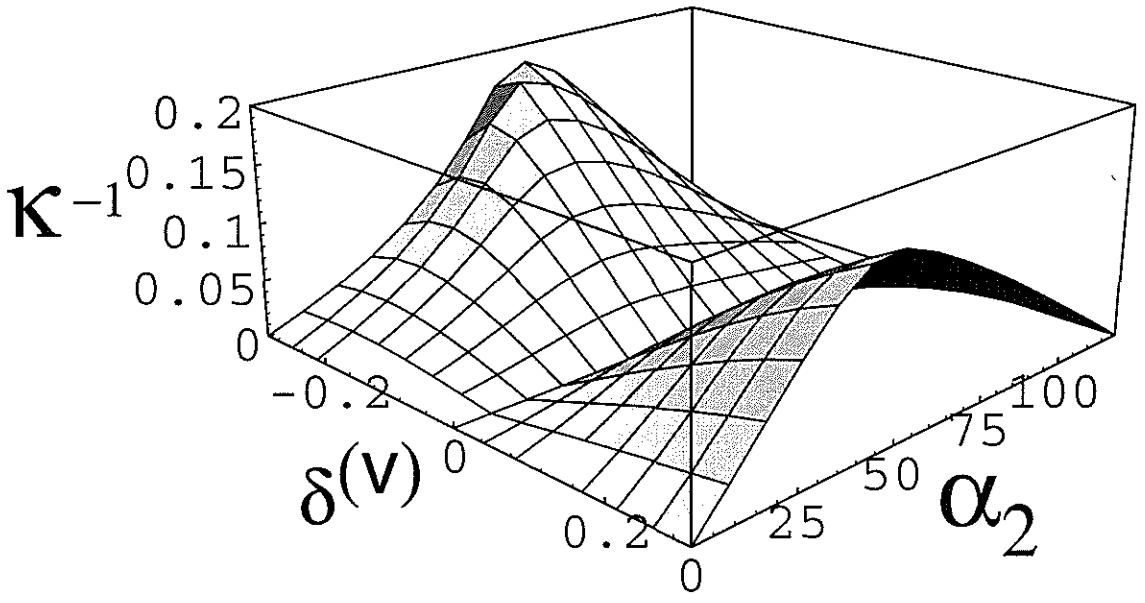

Figure 2: The reciprocal of the condition number (κ^{-1}) as a function of α_2 and $\delta^{(V)}$; α_1=0° and α_3=120°.

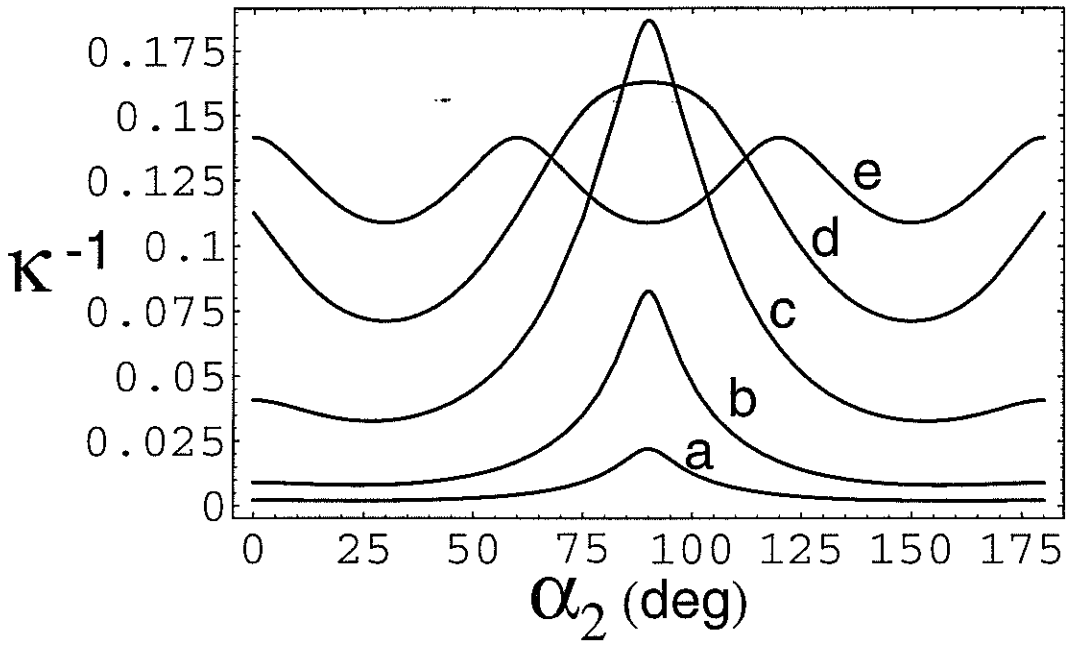

Figure 3: The reciprocal of the condition number (κ^{-1}) as a function of azimuth, α_2, for five different angular separations between three survey lines. Each set of azimuths is rotated so that the middle direction, α_2, spans the azimuths from 0° to 180° measured from the symmetry-axis direction. The five curves correspond to $\Delta\alpha$ = 7.5° (a), 15° (b), 30° (c), 45° (d), and 60° (e); $\delta^{(V)}$=-0.2.

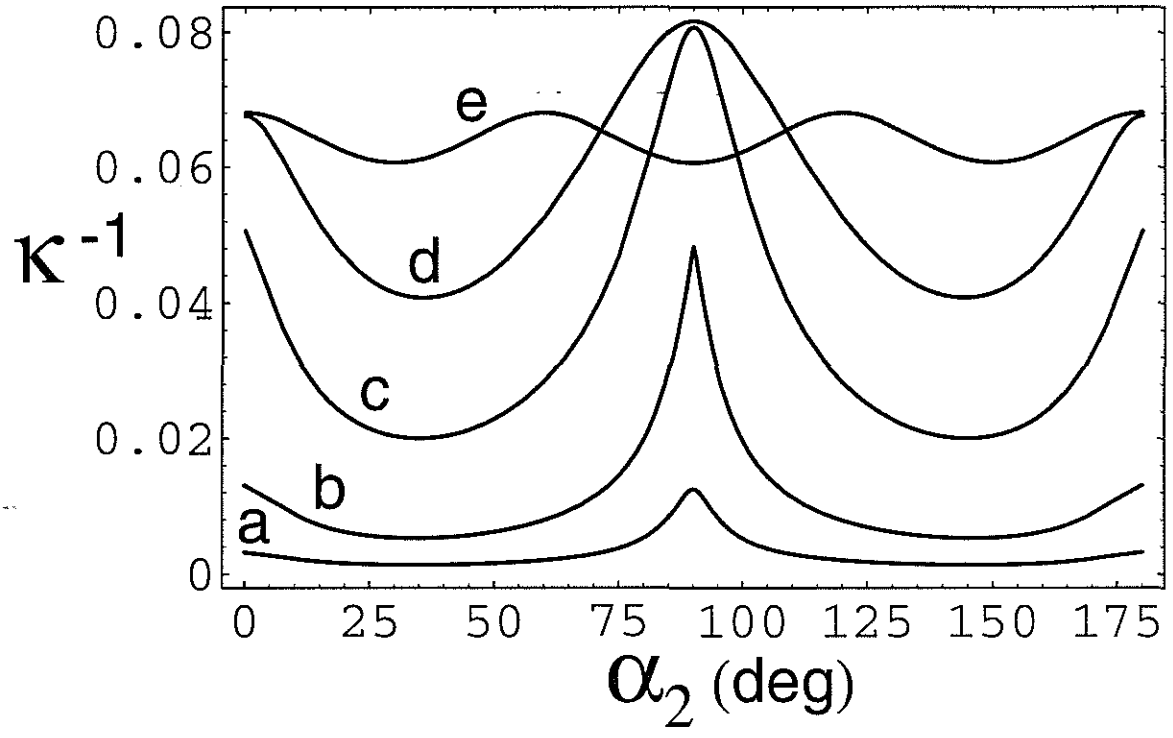

Figure 4: The reciprocal of the condition number κ^{-1} as a function of azimuth α_2 (same as in Figure 3, but for $\delta^{(V)}$=-0.1).

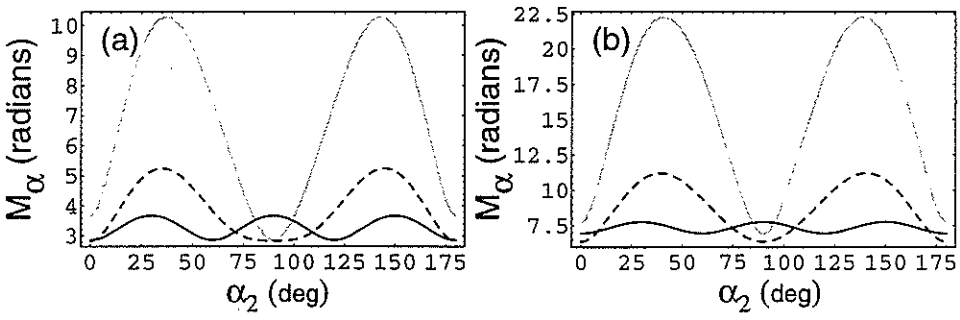

Figure 5: Magnification factor in the absolute error in α measured in radians (α component in the diagonal of $[J^T J]^{-1/2}$) as a function of central azimuth α_2 for three different angular separations $\Delta\alpha$ between survey direction. The three sets of azimuth combinations are rotated so that the central azimuth spans azimuths from 0° to 180° measured from the symmetry-axis direction. The three curves in (a) correspond to angular separations of 30° (gray), 45° (dashed black), and 60° (solid black); $\delta^{(V)}$=-0.2. The three curves in (b) correspond to the same test as in (a), but for $\delta^{(V)}$=-0.1.

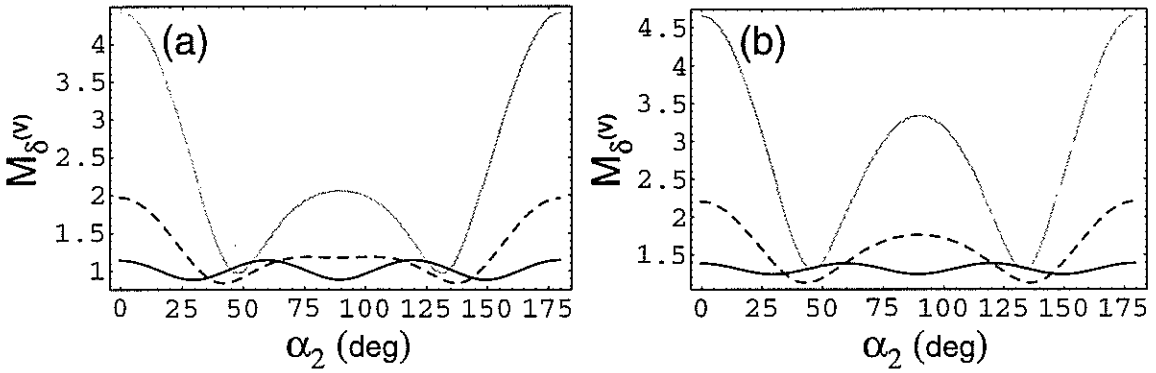

Figure 6: The same as Figure 5, but for the absolute error in $\delta^{(V)}$ ($\delta^{(V)}$ component in the diagonal of $[J^T J]^{-1/2}$). The vertical axis is dimensionless.

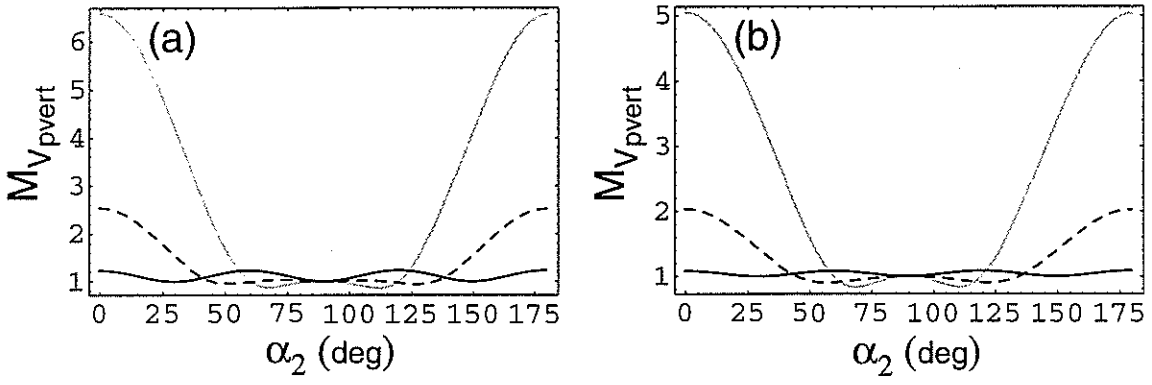

Figure 7: The same as Figures 5 and 6, but for the relative error in V_{Pvert} (V_{Pvert} component in the diagonal of $[J^T J]^{-1/2}$). The vertical axis is dimensionless.

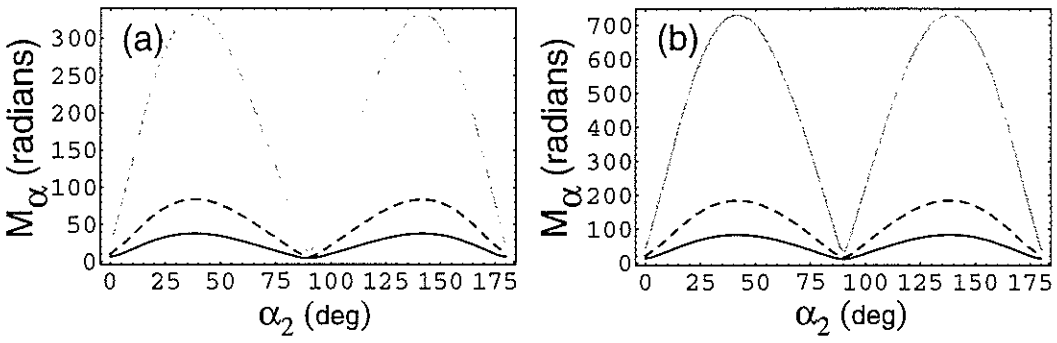

Figure 8: The same as Figure 5, but here the three curves correspond to angular separations of 5° (gray), 10° (dashed black), and 15° (solid black). (a) corresponds to $\delta^{(V)}$=-0.2, while (b) corresponds to $\delta^{(V)}$=-0.1.

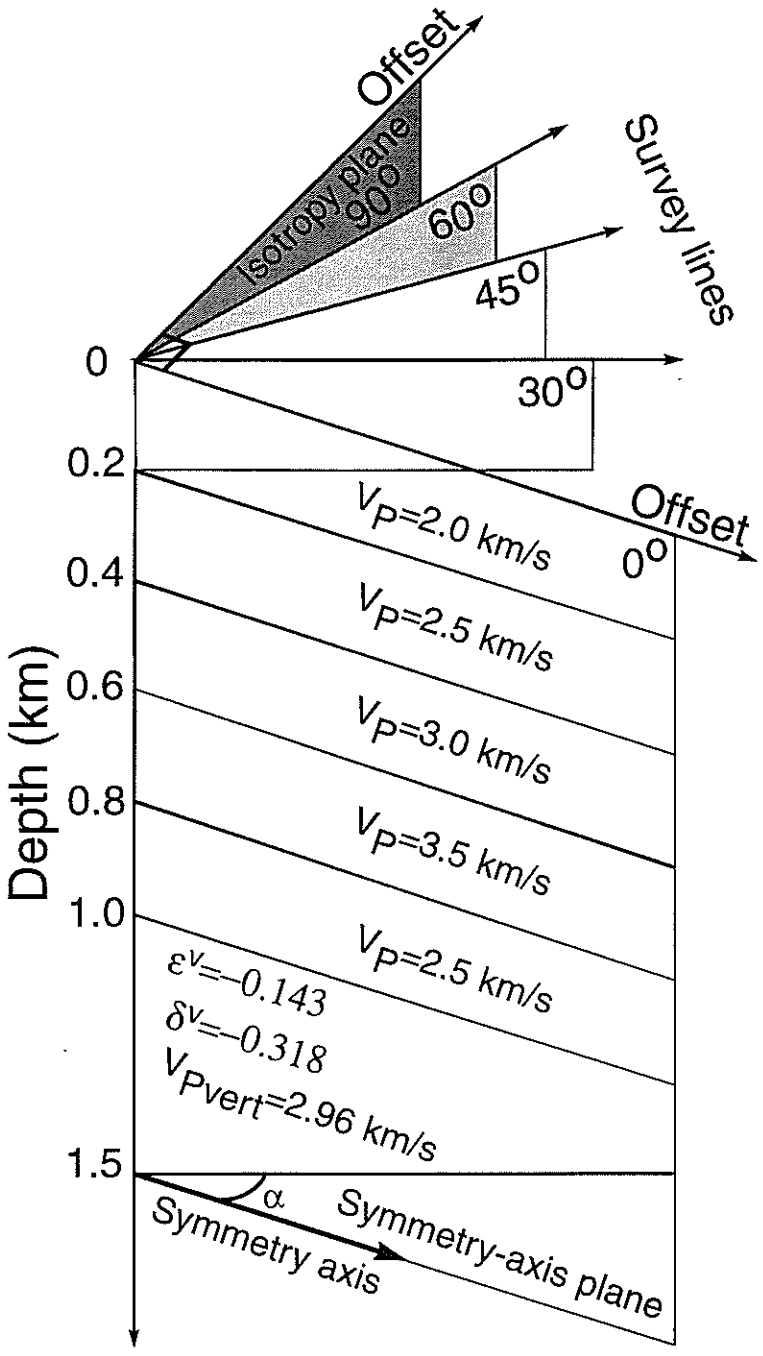

Figure 9: Survey lines over an HTI-layer model which is overlain by five homogeneous isotropic layers.

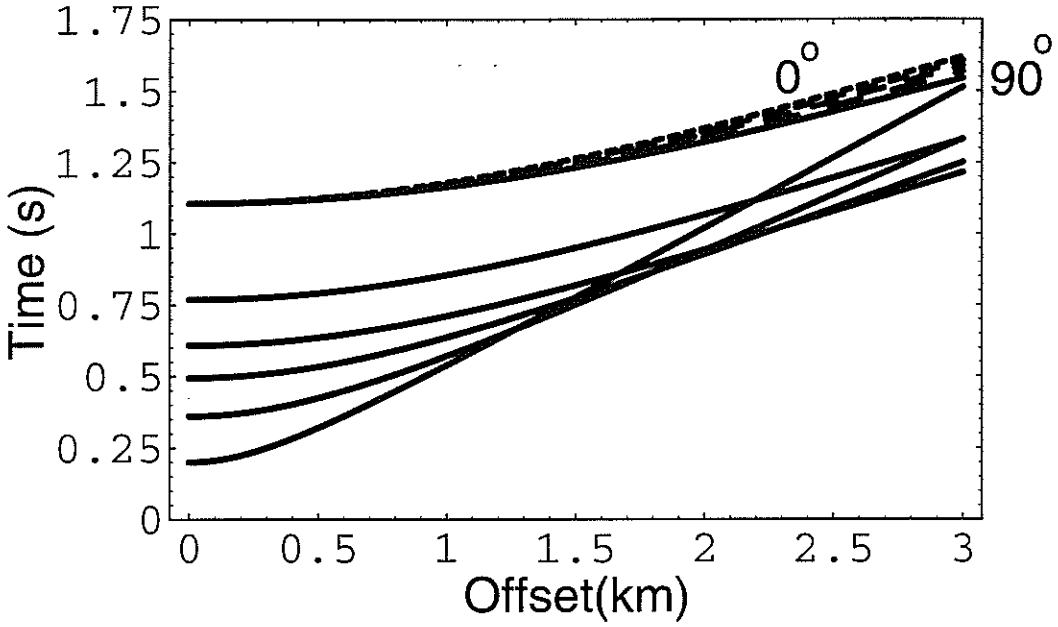

Figure 10: Traveltime-offset curves from all six interfaces of the model in Figure 9 for azimuths α of 0°, 30°, 45°, 60°, and 90°. Note that the reflections from the first five interfaces are azimuthally isotropic, while the reflections from the bottom of the HTI layer are azimuthally anisotropic.

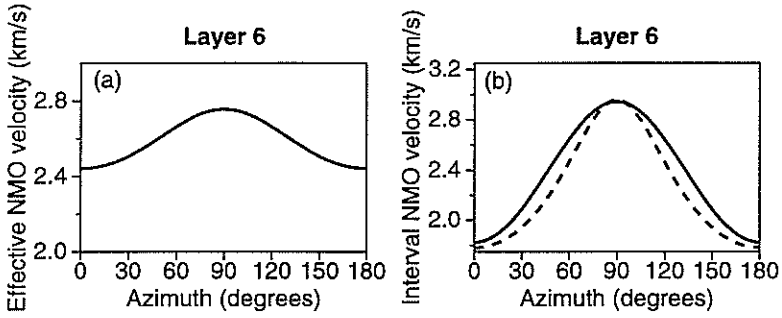

Figure 11: Estimation of interval NMO velocities from synthetic data. (a) shows the azimuthal dependence of the NMO (stacking) velocity obtained from the conventional-spread reflection moveout from the bottom of the HTI layer on the spreadlength equal to the target depth (1.5 km). (b) shows the interval NMO velocity (solid curves) as a function of azimuth computed for the HTI layer using Dix differentiation, and the exact interval NMO velocity (dashed curves) from equation (1). The model geometry and parameters are given in Figure 9. The effective NMO velocity at the top of the HTI layer, estimated from reflection moveout, is 2.67 km/s.

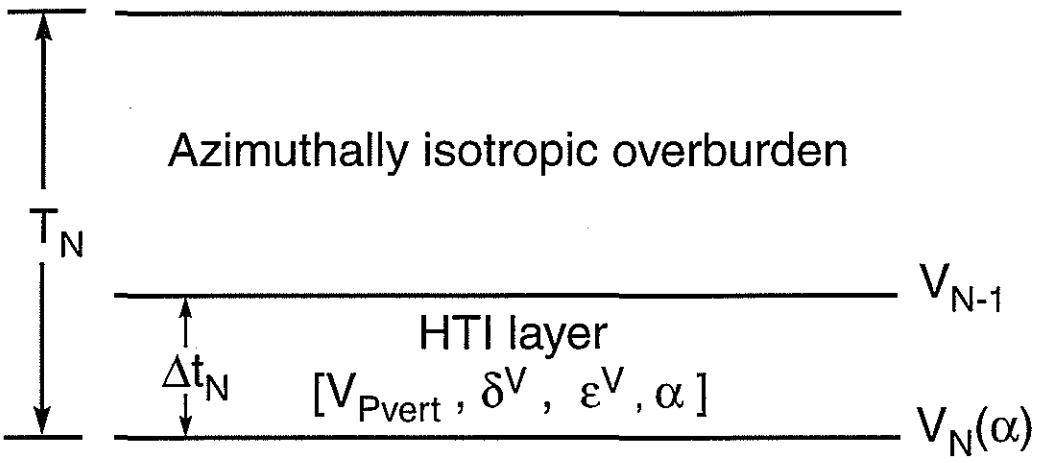

Figure 12: Schematic time section showing a model that contains an azimuthally isotropic overburden over an HTI layer. Δt_N is the two-way vertical traveltime in the HTI layer. The total two-way traveltime to the bottom of the HTI layer is T_N, while the NMO (stacking) velocity at the top and bottom of the HTI layer is denoted as V_{N-1} and V_N, respectively. The ratio $\Delta t_N/T_N = \rho$.

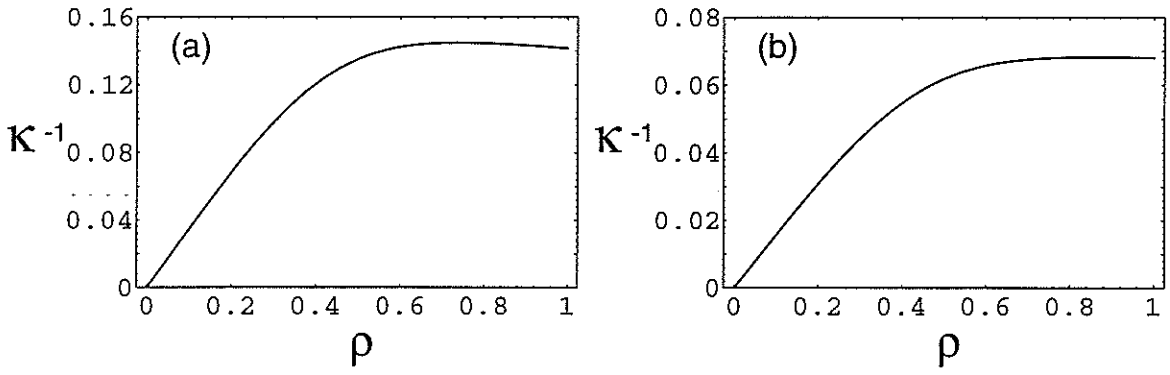

Figure 13: Plot of κ^{-1} as a function of ρ for $V_{\mathrm{N}-1} = 2.0$ km/s, $V_{\mathrm{Pvert}} = 3.0$ km/s. (a) corresponds to $\delta^{(\mathrm{V})} = -0.2$, while (b) corresponds to $\delta^{(\mathrm{V})} = -0.1$. The azimuths are $\alpha_1 = 0°, \alpha_2 = 60°$, and $\alpha_3 = 120°$.

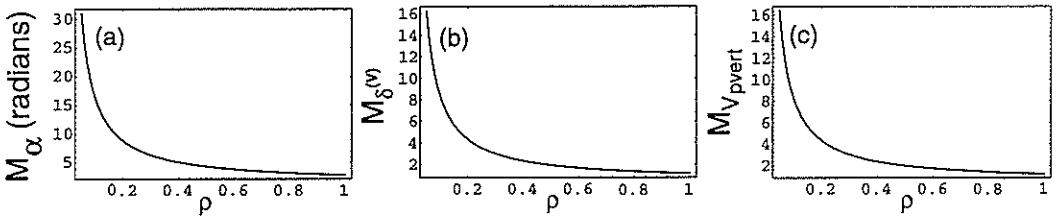

Figure 14: Magnification factors in (a) the absolute error in α measured in radians, (b) the absolute error in $\delta^{(V)}$, and (c) the relative error in V_{Pvert} as a function of the layer-thickness ratio, ρ. The selected survey-line azimuths are: $\alpha_1 = 0°$, $\alpha_2 = 60°$, and $\alpha_3 = 120°$. The model parameters are $V_{N-1} = 2.0$ km/s, $V_{Pvert} = 3.0$ km/s, and $\delta^{(V)} = -0.2$.

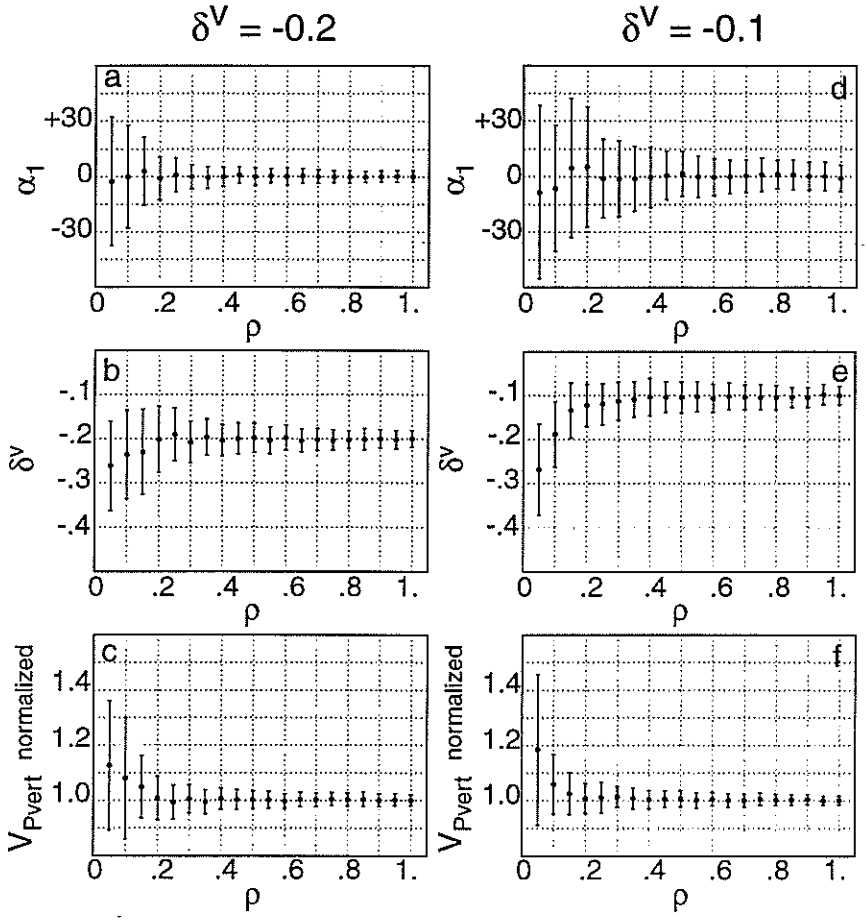

Figure 15: Estimated $V_{\mathrm{Pvert}}, \delta^{\mathrm{V}}$, and the azimuth of the symmetry-axis (α_1), as well as the associated error bars as functions of ρ. The plots in the left column correspond to $\delta^{(\mathrm{V})} = -0.2$, while those in the right correspond to $\delta^{(\mathrm{V})} = -0.1$. $V_{\mathrm{N}-1} = 2.0$ km/s, $V_{\mathrm{Pvert}} = 3.0$ km/s. The azimuths are $\alpha_1 = 0°, \alpha_2 = 60°$, and $\alpha_3 = 120°$. The black dots and error bars represent the computed mean and standard deviation, respectively. The solutions for V_{Pvert} are normalized by the true vertical velocity (3.0 km/s).